Available online at www.sciencedirect.com
ScienceDirect
Journal of Power Sources 171 (2007) 718–727
JOURNAL OF POWER SOURCES
www.elsevier.com/locate/jpowsour

Effects of temperature on the location of the gas–liquid interface in a PEM fuel cell

Chun-I Lee, Hsin-Sen Chu *

Department of Mechanical Engineering, National Chiao Tung University, Hsinchu 300, Taiwan, ROC

Received 31 May 2007; accepted 5 June 2007
Available online 19 June 2007

Abstract

The objective of this study is to investigate the location of the gas–liquid interface at various temperatures in a polymer electrolyte membrane fuel cell under non-isothermal conditions. A mathematical model, coupled with the electrochemical process, two-phase flows, species transfer, and heat transfer is employed. A finite volume-based CFD approach is applied to investigate the species transport behavior in a fuel cell. The effects of two model parameters, namely cell temperature (T_{cell}) and humidification temperature (T_h), on the gas–liquid interface and cell performance are presented. Simulation results indicate that variations of these two parameters influence the location of the gas–liquid interface, the cell performance, and the distribution of liquid water saturation. At lower cell temperatures, the gas–liquid interface moves toward the inlet port of the channel when the humidification temperature is greater than the cell temperature. Therefore, the cell performance decreases as the liquid water clogs the passage for the transport of oxygen. Furthermore, these two factors are closely related to the membrane temperature distribution. Obvious variations in magnitude are seen at a cell temperature of 323 K and a humidification temperature of 343 K.

Keywords: PEM fuel cell; Gas–liquid interface; Temperature; Two-phase system; Performance

1. Introduction

Proton exchange membrane (PEM) fuel cells are currently regarded as promising energy-conversion devices for the 21st century because of their high efficiency, low emission, and quick start-up capability, making them suitable as power supplies of mobile, stationary, and portable devices. However, cell performance is determined by several factors, including the geometry and morphology of transport components, as well as the operating conditions such as pressure, temperature, and humidification of the reactant gases [1–3].

The transport behavior in a fuel cell involves fluid flow, thermal transfer, and mass transport processes, along with the electrochemical reaction. Furthermore, water and heat management are critical to the proper operation of PEM fuel cells. A complex two-phase transport process prevails due to the production of water by oxygen reduction in the cathode catalyst layer. Excess liquid water may block the gas pore paths for mass transport through the porous medium, substantially reducing the reactant transfer rate to the reaction sites and thereby degrading cell performance. However, the formation of liquid water depends on the saturation vapor pressure, which is strongly dependent on the temperature. Therefore, the temperature factor is an inevitable consideration in water management investigations because the phase change of water such as condensation and/or evaporation closely relates to the corresponding saturation pressure [4,5].

Several models have been developed to demonstrate the influence of liquid water on water management. Wang et al. [6] first studied two-phase flow and liquid water transport on the cathode side of a PEM fuel cell based on the multiphase mixture model (M^2 model) originally developed by Wang and Cheng. The model encompassed both single- and two-phase regimes corresponding to low and high current densities and was capable of predicting the transition between these two regimes. The half cell including the gas channel, gas diffusion layer, and catalyst layer on the cathode side of a PEM fuel cell was considered and an expression for calculating the gas–liquid interface was presented in the article. Later, this model was further developed to include a complete cell by You and Liu [7]. Pasaogullari and Wang

* Corresponding author. Tel.: +886 3 5712171x55141.
E-mail address: hschu@cc.nctu.edu.tw (H.-S. Chu).

0378-7753/$ – see front matter © 2007 Elsevier B.V. All rights reserved.
doi:10.1016/j.jpowsour.2007.06.019

Nomenclature

A	specific electrochemically active area
a	water activity
C	molar concentration (mol m^{-3})
C_F	quadratic drag factor
C_P	constant-pressure heat capacity (J kg^{-1} K^{-1})
D^c	capillary diffusion coefficient
D_{ij}	binary diffusion coefficient (m^2 s^{-1})
F	Faraday constant (C mol^{-1})
g	gravitational acceleration (m s^{-2})
h	enthalpy (J kg^{-1})
i	current density (A m^{-2})
j	transfer current density (A m^{-3})
K	permeability (m^2)
k	thermal conductivity (W m^{-1} K^{-1})
M	molecular weight (kg mol^{-1})
P^c	capillary pressure
P	pressure (atm)
R	universal gas constant (J mol^{-1} K^{-1})
r	rate constant
S	source term
s	liquid water saturation
T	temperature (K)
T_{cell}	cell temperature (K)
T_h	humidification temperature (K)
$\vec{u}$	fluid velocity (m s^{-1})
w	mass fraction
x	molar fraction

Subscripts

a	anode
c	cathode
con	condensation
e	electron
eva	evaporation
eff	effective value
g	gas phase
l	liquid phase
p	proton
sat	saturation value
w	water

Superscripts

ref	reference value

Greek

α	transfer coefficient
ε	porosity
ϕ	phase potential (V)
η	overpotential (V)
κ	proton conductivity (S m^{-1})
λ_k	mobility of phase k
μ	dynamic viscosity (N s m^{-2})
ν	kinematic viscosity (m^2 s^{-1})
θ_c	contact angle
ρ	density (kg cm^{-3})
ρ_k	kinetic density (kg m^{-3})
σ	electrical conductivity (S m^{-1})
κ_{eff}	ionic conductivity of the membrane (Ω^{-1} m^{-1})
τ	tortuosity of the porous medium
ξ	stoichiometric flow ratio
ψ	membrane water content
ζ	surface tension (N m^{-1})

[8] developed a model to explore the two-phase flow physics in the cathode gas diffusion layer. The simulations revealed that flooding of the porous cathode reduced the rate of oxygen transport to the cathode catalyst layer. Furthermore, they indicated that the humidification level and the flow rate of reactant streams are key parameters controlling PEM fuel cell performance, two-phase flow, and transport characteristics. Meng and Wang [9] improved their three-dimensional model based on recent visualization experiments, and more accurately investigated the two-phase behavior under different gas utilizations. Although energy transport was ignored, their model was able to predict liquid water flooding dynamics. Luo et al. [10] presented a three-dimensional, two-phase isothermal model based on the M^2 formulation for investigating the condensation and/or evaporation interface under the condition of low-humidity inlet reactant gases, and they successfully predicted the important feature of the dry-wet-dry transition (DET) in the PEM fuel cell.

Zhang et al. [11] studied liquid water transport and its removal from the gas diffusion layer and gas channel of PEM fuel cells both experimentally and theoretically. The distribution of liquid water on the gas diffusion layer surface and inside the gas channel was observed *in situ*. They characterized the formation and emergence of liquid water from the gas diffusion layer surface and identified two modes of liquid water removal from the gas diffusion layer surface. Ju et al. [12] presented the first work in which a mathematical model of the energy equation was systematically derived from thermodynamics. The thermal model was further coupled with the electrochemical and mass transport to deal with the heat and water management in PEM fuel cells. Later, Wang and Wang [13] expanded the M^2 model to permit investigation of the interaction between the two-phase flow and thermal transport due to non-isothermal effects. The results revealed that vapor-phase diffusion enhances water removal and provides a new mechanism for heat removal through a phase change process. This new heat removal mechanism is similar to the heat pipe effect. Shimpalee and Dutta [14] presented a mathematical model to predict the temperature distribution inside a straight-channel PEM fuel cell and to study the effect of heat produced by the electrochemical reactions on fuel cell performance. Source terms for transport equations, heat generation, and a phase change model were presented to facilitate their modeling work. The results showed that the temperature profiles depend on the generation of heat by electrochemical reactions and phase changes of water inside the fuel cell. Further, the

cell performance is not merely influenced by the inlet humidity conditions, cell voltage, and membrane thickness, but also by the temperature rise within the fuel cell. Natarajan and Nguyen [15] developed a pseudo-three-dimensional model by extending a two-dimensional isothermal model for conventional flow fields. Their results indicated that water removal by evaporation increases at higher temperatures and at higher stoichiometric flow rates, which results in better cell performance. However, if the water produced by the electrochemical reaction cannot be effectively removed from the cathode side, then flooding of the electrode will occur, reducing access of the reactants to the catalyst layer. Yang et al. [16] reported on the mechanics of liquid water transport; starting from emergence on the gas diffusion layer surface, droplets grow and move toward the mainstream flow in the gas channels. Furthermore, the oversaturated water vapor causes more liquid film formation on the hydrophilic channel walls and the consequent channel clogging affects cell performance. Liu et al. [17] studied experimentally the two-phase flow of reactants and products as well as the water flooding situation in the gas flow channel of a cathode in a PEM fuel cell with three flow fields. Their study addressed the effects of flow field, cell temperature, cathode gas flow rate, and operation time on water build-up and cell performance. The results indicated that liquid water forms in columns that accumulate in the cathode flow channels and clogs the porous medium, limiting mass transfer, thereby resulting in degraded cell performance. Further, the amount of water in the flow channels at high temperature is much less than that at low temperature.

The above literature review clearly indicates that water and thermal management are critical issues in investigations of PEM fuel cells. However, discussions concerning the effect of the gas–liquid interface on the cell performance and transport process are rarely seen. Therefore, in this study, we report the formation and influence of the gas–liquid interface along the flow channel direction at various cell temperatures and humidification temperatures using a non-isothermal, three-dimensional, multicomponent, two-phase model of a PEM fuel cell. Additionally, the temperature distribution in the cell domain membrane and the distributions of temperature and liquid water saturation in the cross-section of the cathode gas diffusion layer in the inlet region have been investigated. The developed model has been solved by means of commercial computational fluid dynamics software based on the finite volume approach [18–22].

2. Mathematical model

In this study, the multiphase mixture formulation (M^2 model) has been adopted as it is particularly suitable for two-phase flow modeling in PEM fuel cells [6,8–10]. It regards the multiphase system as a chemical mixture and the multiphase flow is then described in terms of a mass-averaged mixture velocity and diffusive flux. The physical model employed in this study consists of nine parts, namely bipolar plates, gas flow channels, gas diffusion layers, and catalyst layers on both the anode and cathode sides, and a polymer membrane that is sandwiched between them, as illustrated in Fig. 1. Symmetry is assumed, and a single straight flow channel is therefore considered herein.

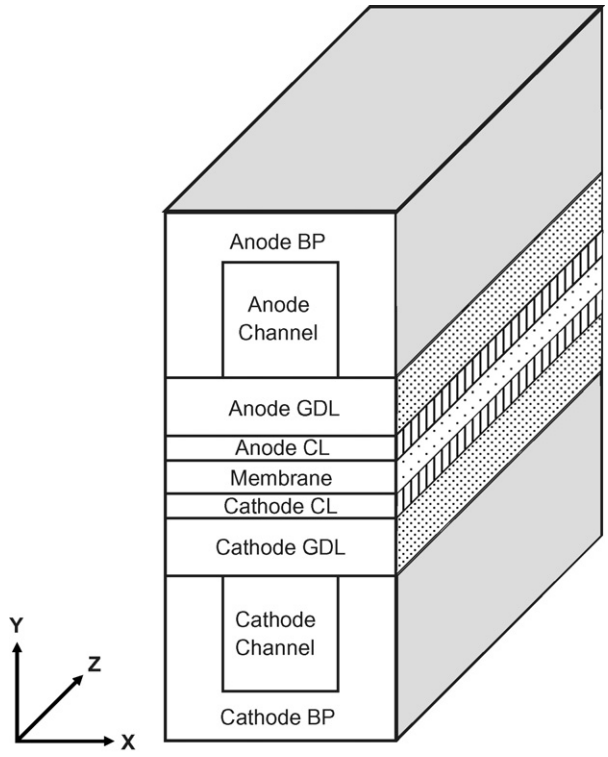

Fig. 1. Schematic structure of PEMFC and computational domain.

Utilizing the M^2 formulation for two-phase transport, the proposed model incorporates the following assumptions.

1. The system operates in a steady state.
2. The gas mixtures at the anode and cathode are ideal gases.
3. The mixture flow field is laminar as its velocity is low under normal operating conditions.
4. The properties of the porous medium are isotropic and homogeneous.
5. The mass source/sink is negligible in the continuity equation [23].
6. The thermal conductivities of the cell components are constant.

2.1. Governing equations

The non-isothermal, three-dimensional, multi-component, and two-phase model of a PEM fuel cell includes five nonlinear coupled conservation equations of mass, momentum, energy, species, and charge, which are described as follows.

2.1.1. Mass conservation equation

Since the gaseous and liquid water are present simultaneously in the control volume, the conservation equation of mass for a multiphase mixture is:

$$\nabla \cdot (\varepsilon_{\text{eff}} \rho \vec{u}) = 0 \tag{1}$$

where ρ represents the density of the mixture and is defined as the volume-weighted average of the phase mass concentration

in the two-phase flow [6]. When liquid water is present, the effective porosity is given by $\varepsilon_{\text{eff}} = \varepsilon(1-s)$.

2.1.2. Momentum conservation equation

The general form of the Navier–Stokes equation is used with source terms that describe the drag forces in the porous medium. The equation is:

$$\nabla\cdot(\rho\varepsilon_{\text{eff}}\vec{u}\vec{u}) = -\varepsilon_{\text{eff}}\nabla P + \nabla\cdot(\varepsilon_{\text{eff}}\mu_{\text{eff}}\nabla\vec{u}) + \varepsilon_{\text{eff}}\rho_k g + S_{\text{m}} \quad (2)$$

where μ_{eff} is the effective viscosity of the mixture, ρ_k the kinetic density, and S_{m} is the sum of the Darcy and the Forchheimer drag forces,

$$S_{\text{m}} = -(\vec{F}_{\text{Darcy}} + \vec{F}_{\text{Forch}}) \quad (3)$$

which are given by:

$$\text{Darcy drag force} = \vec{F}_{\text{Darcy}} = \frac{\varepsilon_{\text{eff}}^2\mu_{\text{eff}}\vec{u}}{K} \quad (4)$$

$$\text{Forchheimer drag force} = \vec{F}_{\text{Forch}} = \frac{\varepsilon_{\text{eff}}^3 C_{\text{F}}\rho}{\sqrt{K}}|\vec{u}|\vec{u} \quad (5)$$

The parameters C_{F} and K represent the quadratic drag factor and the permeability.

2.1.3. Species conservation equation

The species conservation equation for the gas mixture is

$$\nabla\cdot(\varepsilon_{\text{eff}}\vec{u}C_k) = \nabla\cdot(D_{k,\text{eff}}\nabla C_k) + S_{\text{c}} \quad (6)$$

where k represents the chemical species, including hydrogen, oxygen, nitrogen, and water. $D_{k,\text{eff}} = D_k\varepsilon^{\tau}$ represents the effective diffusion coefficient of the kth component of the fuel reactant [24]. The exponent τ on the porosity ε is the tortuosity of the porous medium. The source term S_{c} defines the production or consumption of the kth species in the gas phase and is given by:

$$\text{H}_2 : -\frac{1}{2FC_{\text{a}}}j_{\text{a}} \quad (7)$$

$$\text{O}_2 : -\frac{1}{4FC_{\text{c}}}j_{\text{c}} \quad (8)$$

$$\text{H}_2\text{O} : \frac{1}{2FC_{\text{c}}}j_{\text{c}} \quad (9)$$

The terms j_{a} and j_{c} are defined as:

$$j_{\text{a}} = Aj_0^{\text{ref}}\left(\frac{C_{\text{H}_2}}{C_{\text{H}_2}^{\text{ref}}}\right)\left[e^{(\alpha_{\text{a}}F/RT)\eta} - \frac{1}{e^{(\alpha_{\text{c}}F/RT)\eta}}\right] \quad (10)$$

$$j_{\text{c}} = Aj_0^{\text{ref}}\left(\frac{C_{\text{O}_2}}{C_{\text{O}_2}^{\text{ref}}}\right)\left[e^{(\alpha_{\text{a}}F/RT)\eta} - \frac{1}{e^{(\alpha_{\text{c}}F/RT)\eta}}\right] \quad (11)$$

The above conservation equations of mass, momentum, and species are derived on the basis of the M^2 model. The constitutive relationships of mixture parameter and variables are all dependent on the liquid saturation, defined as the ratio of the liquid volume to the pore volume:

$$s = \frac{V_{\text{l}}}{V_{\text{pore}}} \quad (12)$$

$$\text{Density} : \rho = \rho_{\text{l}}s + \rho_{\text{g}}(1-s) \quad (13)$$

$$\text{Concentration} : \rho C = \rho_{\text{l}}C_{\text{l}}s + \rho_{\text{g}}C_{\text{g}}(1-s) \quad (14)$$

$$\text{Effective porosity} : \varepsilon_{\text{eff}} = \varepsilon(1-s) \quad (15)$$

$$\text{Kinetic density} : \rho_k = \rho_{\text{l}}\lambda_{\text{l}}(s) + \rho_{\text{g}}\lambda_{\text{g}}(s) \quad (16)$$

$$\text{Effective viscosity} : \mu_{\text{eff}} = \frac{\rho_{\text{l}}s + \rho_{\text{g}}(1-s)}{(k_{r\text{l}}/\nu_{\text{l}}) + (k_{r\text{g}}/\nu_{\text{g}})} \quad (17)$$

$$\text{Relative permeability} : \begin{cases} k_{r\text{l}} = s^3, & \text{liquid phase} \\ k_{r\text{g}} = (1-s)^3, & \text{gas phase} \end{cases} \quad (18)$$

$$\text{Relative mobility} : \begin{cases} \lambda_{\text{l}}(s) = \dfrac{k_{r\text{l}}/\nu_{\text{l}}}{k_{r\text{l}}/\nu_{\text{l}} + k_{r\text{g}}/\nu_{\text{g}}}, & \text{liquid phase} \\ \lambda_{\text{g}}(s) = 1 - \lambda_{\text{l}}(s), & \text{gas phase} \end{cases} \quad (19)$$

Furthermore, during the operation of a fuel cell, liquid water forms if the partial pressure of water vapor exceeds the saturation vapor pressure. The liquid water thus formed may occupy the pores and thereby prevent the diffusion of fuel, causing mass transport overpotential in the porous medium. Hence, the effect of liquid water is taken into account. Additionally, capillary forces dominate the transport of liquid water on the hydrophilic surfaces because the pores in the porous medium are extremely small. Therefore, the generalized Richards equation, developed by Wang and Beckermann [25,26] to elucidate two-phase flow transport in capillary porous media, is applied:

$$\nabla\cdot(\varepsilon_{\text{eff}}\rho\vec{u}\lambda_{\text{l}}(s)) = \nabla\cdot\left(\varepsilon_{\text{eff}}D^{\text{c}}\nabla s - \frac{Kk_{r\text{l}}k_{r\text{g}}(\rho_{\text{l}}-\rho_{\text{g}})g}{k_{r\text{l}}\nu_{\text{g}} + k_{r\text{g}}\nu_{\text{l}}}\right) + S_{\text{l}} \quad (20)$$

where D^{c} and P^{c} represent the capillary diffusion coefficient and the capillary pressure, respectively:

$$D^{\text{c}} = -\frac{Kk_{r\text{l}}k_{r\text{g}}(\text{d}P^{\text{c}}/\text{d}s)}{k_{r\text{l}}\nu_{\text{g}} + k_{r\text{g}}\nu_{\text{l}}} \quad (21)$$

$$P^{\text{c}} = \varsigma\cos\theta_{\text{c}}\left(\frac{\varepsilon_{\text{eff}}}{K}\right)^{1/2}J(s) \quad (22)$$

and where $J(s)$ is the Leverett function, which takes the following form [27,28]:

$$J(s) = \begin{cases} 1.417(1-s) - 2.12(1-s)^2 + 1.263(1-s)^3, & \theta_{\text{c}} < 90^0 \\ 1.417s - 2.12s^2 + 1.263s^3, & \theta_{\text{c}} > 90^0 \end{cases} \quad (23)$$

In Eq. (22), the contact angle, θ_c, of the gas diffusion layer is dependent upon the hydrophilic ($0^\circ < \theta_c < 90^\circ$) or hydrophobic ($90^\circ < \theta_c < 180^\circ$) nature of this layer, and varies with the Teflon content. We assume here that the gas diffusion layer is a hydrophilic medium. Further, the surface tension, ζ, for the liquid water–air system is taken as $0.0625\,\mathrm{N\,m^{-1}}$ [27].

S_l is a simplified switch function between condensation and/or evaporation of liquid water under these non-equilibrium conditions [29]. When the partial pressure of water vapor exceeds the saturation pressure of water, liquid water may form and occupy the pores in the porous medium. Conversely, the liquid water will evaporate if the partial pressure of water vapor is less than the saturation pressure of water:

$$S_l = \begin{cases} M_l r_{con} \dfrac{\varepsilon_{eff} x_w}{RT}(x_w P - P_{sat}), & \text{if } x_w P > P_{sat} \\ r_{eva}\varepsilon_{eff} s \rho_l (x_w P - P_{H_2O}), & \text{if } x_w P < P_{sat} \end{cases} \quad (24)$$

where r_{con} and r_{eva} are the condensation and evaporation rate constants, respectively; x_w the molar fraction of water vapor, and P_{sat} is the saturation pressure of water, which varies with temperature [30].

$$\log_{10} P_{sat} = -2.1794 + 0.02953T - 9.1837 \times 10^{-5}T^2 + 1.4454 \times 10^{-7}T^3 \quad (25)$$

2.1.4. Energy equation

The heat generation sources in a PEM fuel cell account for the irreversible heat and entropic heat that is generated by electrochemical reactions, Joule heating that arises from proton/electronic resistance, and the latent heat of water condensation and/or evaporation. A generalized energy conservation equation is:

$$\nabla \cdot (\varepsilon_{eff}\rho C_p \vec{u} T) = \nabla \cdot \left(k_{eff}\nabla T + \sum_{i=1}^{n}\sum_{j=1}^{n-1} \rho D_{ij} \nabla w_j h_i \right) - S_\eta + \frac{|i \cdot i|}{\sigma} + S_T \quad (26)$$

where k_{eff} represents the effective thermal conductivity. On the right-hand side of the equation, the first two terms represent the conduction energy and the reactant enthalpy flux; the third and fourth terms represent electrical-related thermal effects, and the last term is a source term, associated with the phase change.

2.1.5. Charge conservation

In a fuel cell, the potential gradient effect causes electrons and protons to move along individual paths. Solid phases control the movement of electrons. Electron transport generally occurs only in the bipolar plates, the diffusion layers, and the catalyst layers. However, ionomer phases control the motion of protons, which occurs in the catalyst layer and the electrolyte membrane. Potential fields in these two media are described as follows.

For electrons:

$$\nabla \cdot (\sigma_{eff}\nabla\phi_e) + S_{\phi_e} = 0 \quad (27)$$

$$S_{\phi_e} = \begin{matrix} -j_a & \text{at anode} \\ j_c & \text{at cathode} \end{matrix} \quad (28)$$

For protons:

$$\nabla \cdot (\kappa_{eff}\nabla\phi_p) + S_{\phi_p} = 0 \quad (29)$$

$$S_\phi = \begin{matrix} -j_a & \text{at anode} \\ j_c & \text{at cathode} \end{matrix} \quad (30)$$

where σ_{eff}, κ_{eff}, ϕ_e, ϕ_p, S_{ϕ_e} and S_ϕ denote electron conductivity, proton conductivity, electronic phase potential, electrolyte phase potential, and consumption rates of charge and product in the electrochemical reaction in the catalyst layer, respectively.

The membrane conductivity is strongly related to the temperature and the water content ψ. It is defined as the ratio of the number of water molecules to the number of charge sites [30]:

$$\kappa_{eff}(T) = (05139\psi - 0.00326)\exp\left[1268\left(\frac{1}{303} - \frac{1}{T}\right)\right] \quad (31)$$

The water content of the membrane surface depends on the activity of the water vapor, which also depends on the partial pressure of the water. Therefore, the empirical relationship between them can be applied:

$$\psi = \begin{cases} 0.043 + 17.81a - 39.85a^2 + 36.0a^3, & 0 \le a \le 1 \\ 14 + 1.4(a-1), & 1 < a \le 3 \end{cases} \quad (32)$$

$$a = \frac{x_w P}{P_{sat}} \quad (33)$$

2.2. Boundary conditions

Boundary conditions are necessary and crucial for solving the above equations. They describe the operating conditions as well as the model geometry characteristic of the PEM fuel cell. The most important ones are as follows.

Inlet boundaries: the fuel and oxidant flow rates along the flow channel can be described by a stoichiometric flow ratio, ξ, which is defined as the amount of reactant in the chamber gas feed divided by the amount that is required by the electrochemical reaction [20]. The inlet molar concentrations are determined by the inlet pressure, the temperature, and the humidity, according to the ideal gas law.
Outlet boundaries: fully developed flow is applied.
Walls: Neumann conditions and no-slip conditions are applied.
Symmetric boundaries: mass flux or momentum flux has zero gradients.
Electronic phase potential boundaries: fixed total cell overpotential at the outer boundary of the cathode is specified.

$$\begin{cases} \phi_e = 0 & \text{at anode bipolar plate} \\ \phi_e = \eta_{cell} & \text{at cathode bipolar plate} \\ \dfrac{\partial \phi_e}{\partial y} = 0 & \text{elsewhere} \end{cases} \quad (34)$$

Table 1
Geometrical and operating parameters

Quantity	Value	Sources
Gas channel depth/width	0.762/0.762 mm	
Shoulder width	0.381 mm	
GDL thickness	0.3 mm	
Catalyst layer thickness	0.01 mm	
Membrane thickness	0.03 mm	
Fuel cell height/length	1.534/71.12 mm	
Anode/cathode pressure	1/1 atm	
Stoichiometry, at ξ_a/ξ_c at 1.0 A cm^{-2}	1.5/3	[32]
Relative humidity of anode/cathode inlet	100/100%	
Porosity of diffusion and catalyst layers	0.4/0.4	[33]
Porosity of membrane	0.28	[33]
Permeability of diffusion and catalyst layers	$1.76 \times 10^{-11}/1.76 \times 10^{-11}$ m^2	[34]
Permeability of membrane	1.8×10^{-18} m^2	[34]
Transfer coefficient at anode/cathode	0.5/1.5	[34]
Condensation rate constant	100 s^{-1}	[24]
Evaporation rate constant	100 atm^{-1} s^{-1}	[24]
Tortuosity of the diffusion and catalyst layers	1.5	[34]
Tortuosity of the membrane	3	[34]
Surface tension (ζ)	0.0625 N m^{-1}	[27]

2.3. Numerical procedures

The governing equations with their related boundary conditions were solved using a commercial code based on the SIMPLE algorithm for convection-diffusion problems. Details of the numerical solution procedure and the code are presented elsewhere [4,21,22]. The geometrical and operating parameters of the PEM fuel cell are presented in Table 1. In the simulation, a uniform grid distribution is used to calculate the complex electrochemical reaction and physical phenomena in the fuel cell. The numbers of grid nodes used for the model were 17 in the x-direction, 51 in the y-direction, and 71 in the z-direction. A grid dependence test was carried out to make sure that the solution obtained was independent of the grid density used. As a convergence criterion it was imposed that the normalized residual for each model variable is smaller than 10^{-4} [31].

3. Results and discussion

In this study, the non-equilibrium conditions of partial pressure deviation from saturation pressure have been considered. Our quest to delineate the effects of the gas–liquid interface on a PEM fuel cell has involved the following two parts. First, as a preliminary study, the cell temperature and humidification temperature were set as being equal. Second, we considered a scenario whereby cell temperatures were altered at a fixed humidification temperature. For all of the calculations carried out in this paper, the fuel flows were co-flows and inlet stoichiometric ratios of 1.5 and 3 were used for the anode and cathode sides based on a reference current density of 1 A cm^{-2}. Furthermore, fully humidified hydrogen and oxygen were fed to the anode and cathode inlets, respectively.

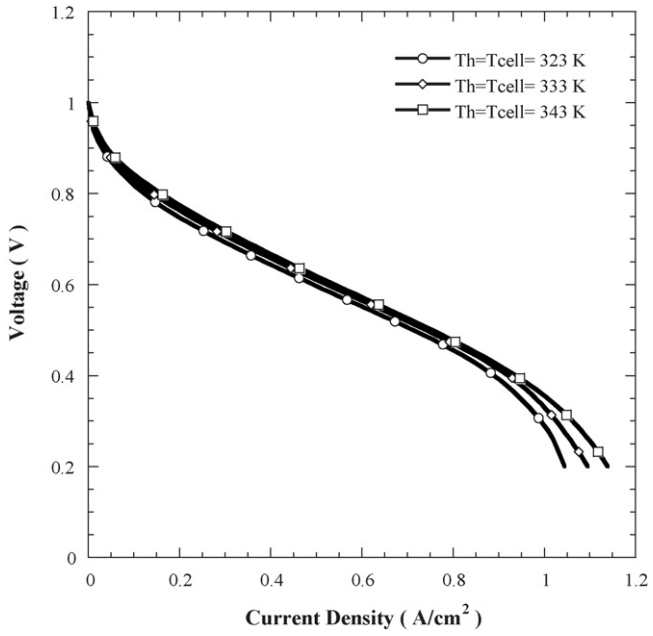

Fig. 2. Polarization curves at various cell temperatures with equal humidification temperature.

Fig. 2 shows the polarization curves of the cell at equal cell and humidification temperatures of 323, 333, and 343 K. The results reveal that the cell performance improves as the temperature is increased because a higher temperature results in higher catalytic activity and a higher capacity for water removal by evaporation. Hence, increasing the temperature is helpful in reducing the level of flooding. Moreover, a higher cell temperature increases the membrane conductivity and mass diffusivity, and decreases the mass transport resistance. Fig. 3 presents the effect of temperature on the location of the interface at which liquid water begins to condense along the cathode flow channel at a cell voltage of 0.7 V. Indeed, the interface is defined as the location where the liquid water begins to condense, and so the saturation value behind this interface is greater than zero and this gives rise to the two-phase flow region. The horizontal

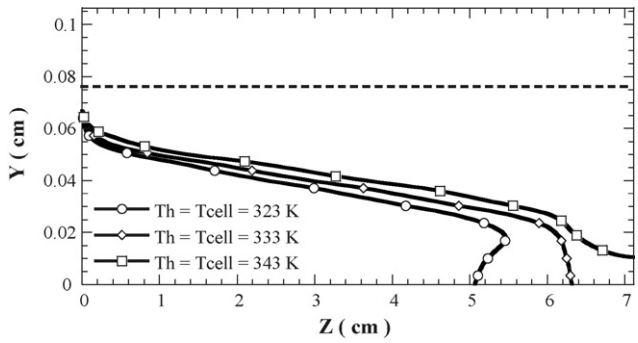

Fig. 3. Effect of cell temperature on the location of the interface where liquid water begins to condense along the flow channel at a cell operating voltage of 0.7 V.

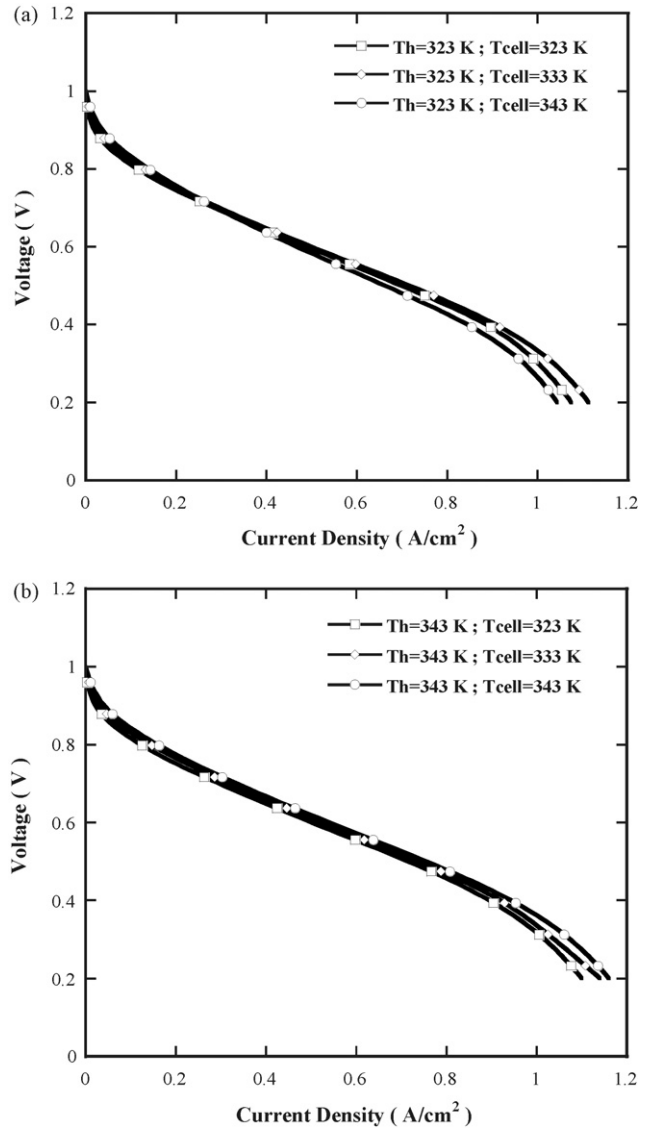

Fig. 4. Polarization curves for various cell temperatures at: (a) $T_h = 323$ K and (b) $T_h = 343$ K.

dotted line indicates the interface between the flow channel and the gas diffusion layer of the cathode. The results reveal that the gas–liquid interface moves toward the flow channel inlet as the temperature is decreased, because the formation of liquid water depends on the saturation pressure, which is strongly dependent on the temperature. Liquid water is more easily and quickly condensed at a lower temperature. Additionally, the formation of liquid water may block pore paths for mass transport through the porous diffusion layer to the catalyst layer, thereby reducing cell performance. An increase in temperature increases the saturation pressure of water vapor, in turn increasing the evaporation capacity of the gas stream. However, although not shown here, a high temperature may result in the membrane drying out.

In the second part of this study, the effect of cell temperature was investigated for a fixed gas humidification temperature. As the stoichiometric flow ratio and the humidification temperature do not change in this phase of simulation, the reactant flow rates were kept constant. Polarization curves at $T_h = 323$ and 343 K at various cell temperatures are plotted in Fig. 4. The curves in Fig. 4(a) reveal that the cell performance improves as the cell temperature is increased from 323 to 333 K, but deteriorates as the temperature is further increased from 333 to 343 K. This result probably follows from the fact that the humidification temperature is less than the cell temperature, and the inlet fuel gases are therefore unsaturated. Therefore, water is almost entirely present in vapor form. Accordingly, the mass fraction of water vapor increases along the channel because of evaporation of liquid water from the catalyst layer. Hence, a high temperature reduces the water content of the membrane, dehydrating it, and reducing its ionic conductivity. Fig. 4(b) indicates the positive effect of cell temperature on cell performance. Since the humidification temperature exceeds the cell temperature, liquid water forms when the inlet gases enter the channel. Some of the liquid water keeps the membrane moist and improves its ionic conductivity. Accordingly, the cell performance improves as the cell temperature is increased.

Some experimental investigations [35–37] have demonstrated that the best working conditions for the single cell are those under which the humidification temperature slightly exceeds the cell temperature. The objective of this study has been to investigate the impact of the formation of liquid water on cell performance. Therefore, the case in which the humidification temperature exceeds the cell temperature has been considered. Fig. 5(a and b) show the location of the gas–liquid interface along the flow channel at a cell operating voltage of 0.7 V and a humidification temperature of 343 K as the cell temperature is varied. The results reveal that the gas–liquid interface gradually moves to the gas inlet as the cell temperature is decreased, which

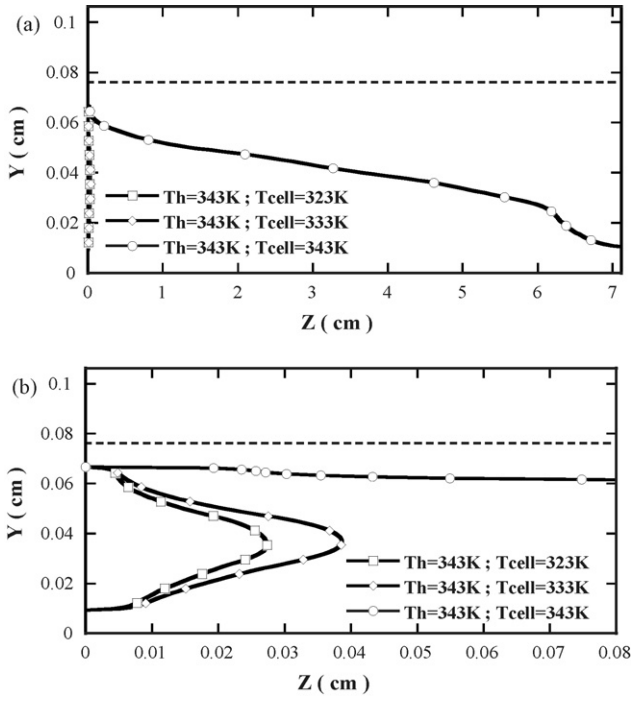

Fig. 5. Effects of cell temperature on the location of the interface where liquid water begins to condense along the flow channel at a cell operating voltage of 0.7 V and a humidification temperature of 343 K. (a) Z = 0–7.112 cm and (b) Z = 0–0.08 cm.

may be ascribed to the following two reasons. (1) Reducing the cell temperature reduces the saturation pressure, increasing the amount of liquid water generated, shifting the gas–liquid interface closer to the gas channel inlet. (2) Some of the water produced in the cathode catalyst layer by the electrochemical reaction is evaporated because the cell temperature is higher and, therefore, the gas–liquid interface moves closer to the catalyst layer. Fig. 5(b) shows an enlarged portion of the curves along the channel from 0 to 0.08 cm. In conclusion, reducing the cell temperature can reposition the gas–liquid interface and cause liquid water to appear, which is detrimental to cell performance, since this water may occupy the pores in the porous medium, reducing the amount of fuel gases that can reach the catalyst layer.

Fig. 6 displays the liquid water saturation field in the gas flow channel and the gas diffusion layer on the cathode side at various cell temperatures. Each of the figures reveals that liquid water saturation increases along the flow channel, because water is generated in the cathode catalyst layer by an electrochemical reaction. Therefore, liquid water may first appear near the interface between the membrane and the cathode catalyst layer close to the channel outlet. Consequently, the liquid water saturation level in the catalyst layer is higher than that in the gas diffusion layer on the cathode side. Liquid water is transported from the catalyst layer towards the gas diffusion layer only by capillary action; when the liquid water has reached the interface between the flow channel and the gas diffusion layer, it is transported along the channel by the drag force arising from the convective flow of gas. Fig. 7 compares the temperature distributions in the membrane from 323 to 343 K. Each of these figures reveals that the temperature distributions in the membrane gradually decline along the flow channel, and that the distribution is symmetric about the z-center line. Since the inlet gas is fully humidified, the rate of the reaction and the temperature are higher at the inlet. The temperature variation involves

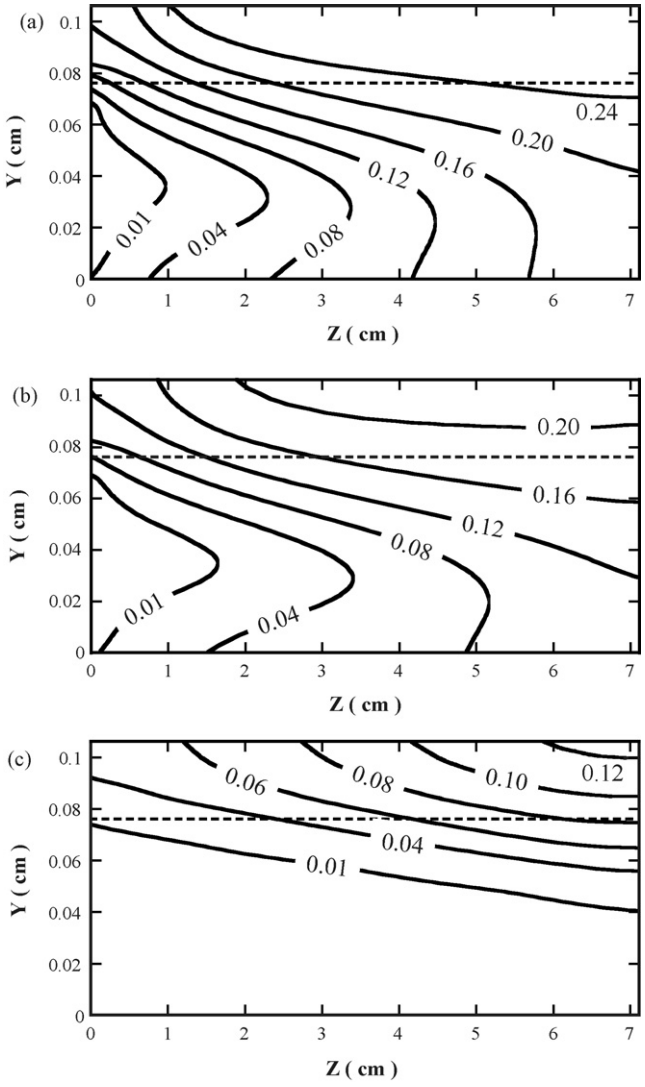

Fig. 6. Liquid water saturation field in the cathode gas channel and diffusion layer along the flow channel at a cell voltage of 0.7 V and a humidification temperature of 343 K. (a) T_{cell} = 323 K, (b) T_{cell} = 333 K, and (c) T_{cell} = 343 K.

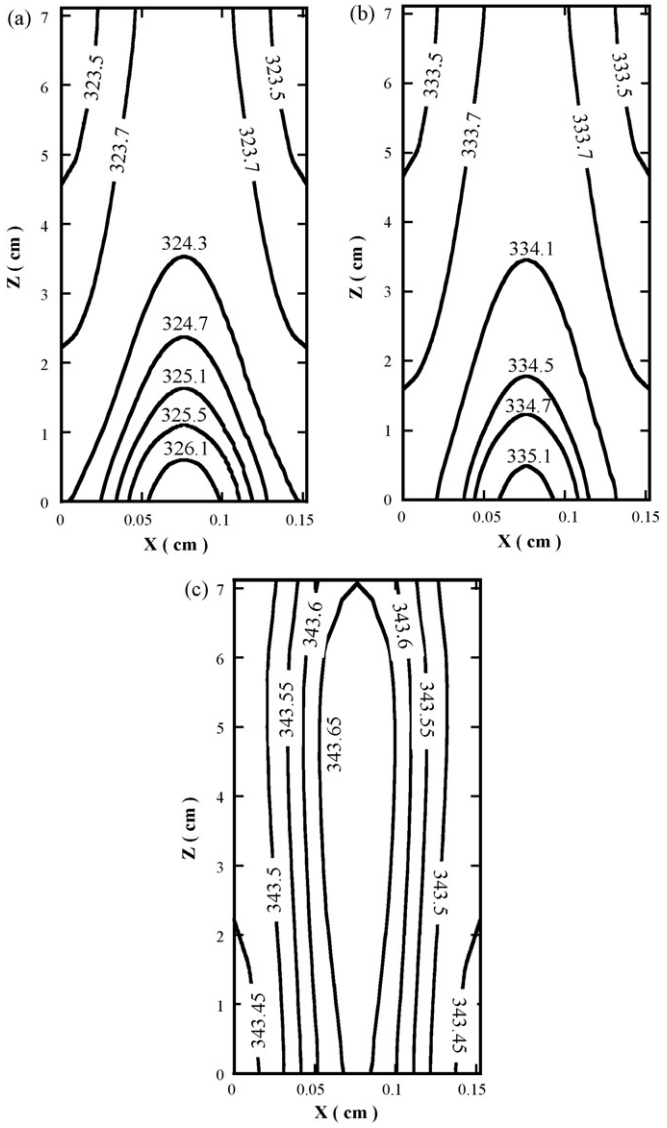

Fig. 7. Temperature contours in the membrane at a cell voltage of 0.7 V and a humidification temperature of 343 K. (a) T_{cell} = 323 K, (b) T_{cell} = 333 K, and (c) T_{cell} = 343 K.

irreversible heat, entropic heat, Joule heating, and latent heat. Additionally, the degree of temperature variation in the membrane is greater when there is a larger difference between the cell temperature and the humidification temperature.

Figs. 8 and 9 show plots of the distributions of liquid water saturation and temperature in the X–Y section of the cathode gas diffusion layer in the inlet region at a cell voltage of 0.7 V and a humidification temperature of 343 K at various cell temperatures. Fig. 8 reveals that the liquid water saturation increases under the land and that the amount of liquid water decreases as the cell temperature is increased. In the gas diffusion layer, two transport mechanisms operate—gas-phase diffusion as a result of the concentration gradient from the channel to the land and liquid water transport by capillary forces from the land to the channel. The liquid water cannot be discharged by the land, so the liquid water saturation on the land is higher than that in the channel. Additionally, the amount of liquid water decreases as

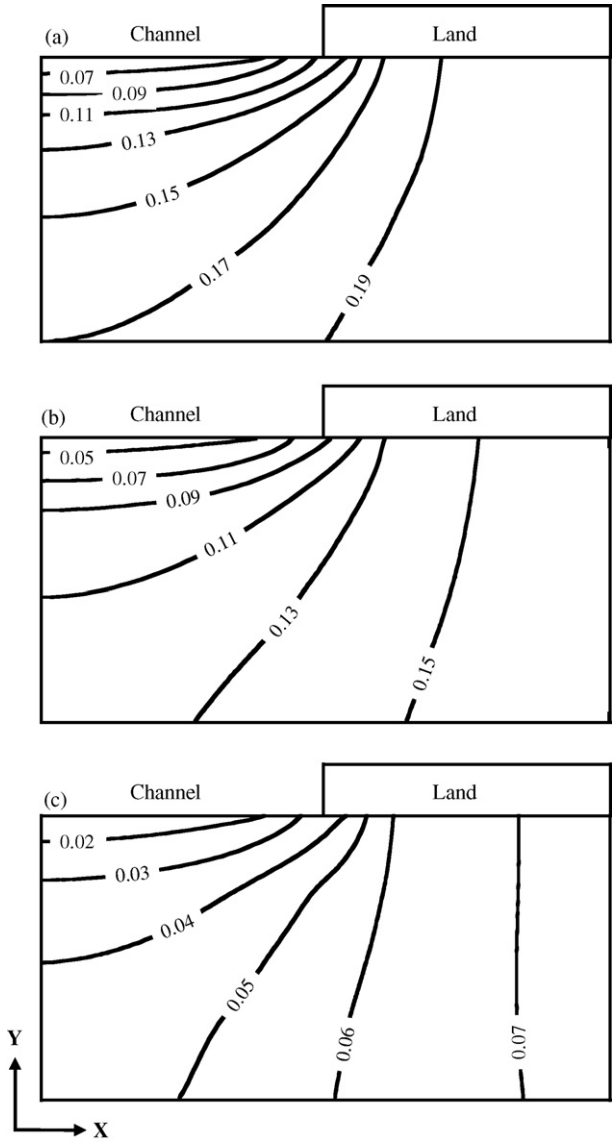

Fig. 8. Liquid water saturation distributions in a cross-section of the cathode gas diffusion layer in the inlet region at a cell voltage of 0.7 V and a humidification temperature of 343 K. (a) T_{cell} = 323 K, (b) T_{cell} = 333 K, and (c) T_{cell} = 343 K.

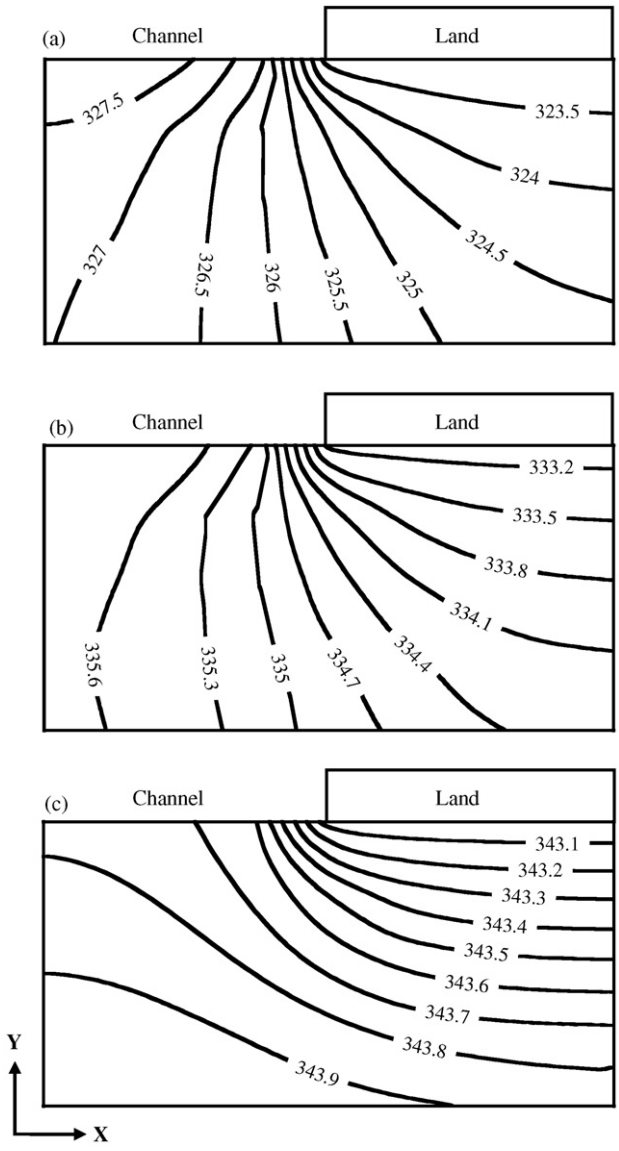

Fig. 9. Temperature distribution in a cross-section of the cathode gas diffusion layer in the inlet region at a cell voltage of 0.7 V and a humidification temperature of 343 K. (a) T_{cell} = 323 K, (b) T_{cell} = 333 K, and (c) T_{cell} = 343 K.

the cell temperature is increased because the saturation pressure increases. Fig. 9 shows that the temperature gradually decreases from the channel to the land. This result has two explanations. (1) Gas-phase diffusion occurs from the channel area to the land; (2) heat produced in the cathode catalyst layer by the electrochemical reaction causes the temperature gradient. Additionally, the degree of temperature variation is greater when there is a larger difference between the cell temperature and the humidification temperature.

4. Conclusions

A three-dimensional, non-isothermal, multi-component, and two-phase mathematical model has been developed in the framework of the computational fluid dynamics code. The effects of temperature on the location of the gas–liquid interface have been

investigated. According to the presented results and the analysis, when the anode and cathode humidification temperatures are equal to or higher than the cell temperature, the gas–liquid interface moves toward the flow channel inlet as the temperature is decreased. Since the formation of liquid water may block pore paths for mass transport through the porous diffusion layer to the catalyst layer, cell performance is reduced. An increase in temperature increases the saturation pressure of water, in turn increasing the evaporation capacity of the gas stream. The temperature distributions in the membrane gradually decline along the flow channel. The distribution is symmetric about the z-center line because the cell reaction rate and the temperature are higher at the inlet region. Numerical analysis of the results of this study has also shown that gas-phase fluid diffuses from the channel to the land and that the capillary-driven liquid water is transported in the opposite direction. Additionally, the degree of temperature variation is greater when there is a large difference between the cell temperature and the humidification temperature.

References

[1] P. Costamagna, S. Srinivasan, J. Power Sources 102 (2001) 242–252.
[2] P. Costamagna, S. Srinivasan, J. Power Sources 102 (2001) 253–269.
[3] H.S. Chu, C. Yeh, F. Chen, J. Power Sources 123 (2003) 1–9.
[4] M.S. Chiang, H.S. Chu, Proc. IMechE Part A, J. Power and Energy 220 (2006) 42–53.
[5] C.Y. Wang, Chem. Rev. 104 (2004) 4727–4766.
[6] Z.H. Wang, C.Y. Wang, K.S. Chen, J. Power Sources 94 (2001) 40–50.
[7] L. You, H. Liu, Int. J. Heat Mass Transfer 45 (2002) 2277–2287.
[8] U. Pasaogullari, C.Y. Wang, J. Electrochem. Soc. 152 (2) (2005) A380–A390.
[9] H. Meng, C.Y. Wang, J. Electrochem. Soc. 152 (9) (2005) A1733–A1741.
[10] G. Luo, H. Ju, C.Y. Wang, J. Electrochem. Soc. 154 (3) (2007) B316–B321.
[11] F.Y. Zhang, X.G. Yang, C.Y. Wang, J. Electrochem. Soc. 153 (2) (2006) A225–A232.
[12] H. Ju, H. Meng, C.Y. Wang, Int. J. Heat Mass Transfer 48 (2005) 1303–1315.
[13] Y. Wang, C.Y. Wang, J. Electrochem. Soc. 153 (6) (2006) A1193–A1200.
[14] S. Shimpalee, S. Dutta, Numer. Heat Transfer, Part A 38 (2000) 111–128.
[15] D. Natarajan, T.V. Nguyen, J. Power Sources 115 (2003) 66–80.
[16] X.G. Yang, F.Y. Zhang, A.L. Lubawy, C.Y. Wang, Electrochem. Solid-State Lett. 7 (11) (2004) A408–A411.
[17] X. Liu, H. Guo, C. Ma, J. Power Sources 156 (2006) 267–280.
[18] S. Dutta, S. Shimpalee, J.V. Van Zee, J. Appl. Electrochem. 30 (2000) 135–146.
[19] T. Berning, N. Djilali, J. Power Sources 124 (2003) 440–452.
[20] S. Um, C.Y. Wang, J. Power Sources 125 (2004) 40–51.
[21] H.C. Liu, W.M. Yan, C.Y. Soong, F. Chen, J. Power Sources 142 (2005) 125–133.
[22] C.Y. Soong, W.M. Yan, C.Y. Tzeng, H.C. Liu, F. Chen, H.S. Chu, J. Power Sources 143 (2005) 36–47.
[23] Y. Wang, C.Y. Wang, J. Electrochem. Soc. 152 (2005) A445–A453.
[24] W. He, J.S. Yi, T.V. Nguyen, AIchE J. 46 (10) (2000) 2053–2064.
[25] C.Y. Wang, C. Beckermann, Int. J. Heat Mass Transfer 36 (1993) 2747–2758.
[26] C.Y. Wang, P. Cheng, Int. J. Heat Mass Transfer 39 (1996) 3607–3618.
[27] U. Pasaogullari, C.Y. Wang, J. Electrochem. Soc. 151 (3) (2004) A399–A406.
[28] U. Pasaogullari, C.Y. Wang, Electrochim. Acta 49 (2004) 4359–4369.
[29] S. Mazumder, J.V. Cole, J. Electrochem. Soc. 150 (11) (2003) A1510–A1517.
[30] T.E. Springer, T.A. Zawodzinski, S. Gottesfeld, J. Electrochem. Soc. 138 (8) (1991) 2334–2342.
[31] CFD-ACE(U)^{TM} User Manual, CFD Research Corp., Huntsville, AL, 2004.
[32] G. Squadrito, G. Maggio, E. Passalacqua, F. Lufrano, A. Patti, J. Appl. Electrochem. 29 (1999) 1449–1455.
[33] S. Um, C.Y. Wang, K.S. Chen, J. Electrochem. Soc. 147 (12) (2000) 4485–4493.
[34] S. Mazumder, J.V. Cole, J. Electrochem. Soc. 150 (11) (2003) A1503–A1509.
[35] L.R. Jordan, A.K. Shukla, T. Behrsing, N.R. Avery, B.C. Muddle, M. Forsyth, J. Power Sources 86 (2000) 250–254.
[36] T.J.P. Freire, E.R. Gonzalez, J. Electroanal. Chem. 503 (2001) 57–68.
[37] M.G. Santarelli, M.F. Torchio, Energy Convers. Manage. 48 (2007) 40–51.